Vibrational Spectra of α-Amino Acids in the Zwitterionic State in Aqueous Solution and the Solid State: DFT Calculations and the Influence of Hydrogen Bonding

Babur Z. Chowdhry,[†] Trevor J. Dines,*[,‡] Saima Jabeen,[†] and Robert Withnall[§]

School of Science, University of Greenwich at Medway, Central Avenue, Chatham Maritime, Kent ME4 4TB, United Kingdom, Division of Electronic Engineering and Physics, University of Dundee, Dundee, DD1 4HN, United Kingdom and Wolfson Centre for Materials Processing, Brunel University, Uxbridge, Middlesex, UB8 3PH, United Kingdom

Received: April 30, 2008; Revised Manuscript Received: August 12, 2008

The zwitterionic forms of the two simplest α-amino acids, glycine and L-alanine, in aqueous solution and the solid state have been modeled by DFT calculations. Calculations of the structures in the solid state, using PW91 or PBE functionals, are in good agreement with the reported crystal structures, and the vibrational spectra computed at the optimized geometries provide a good fit to the observed IR and Raman spectra in the solid state. DFT calculations of the structures and vibrational spectra of the zwitterions in aqueous solution at the B3-LYP/cc-pVDZ level were found to require both explicit and implicit solvation models. Explicit solvation was modeled by inclusion of five hydrogen-bonded water molecules attached to each of the five possible hydrogen-bonding sites in the zwitterion and the integration equation formalism polarizable continuum model (IEF-PCM) was employed, providing a satisfactory fit to observed IR and Raman spectra. Band assignments are reported in terms of potential-energy distributions, which differ in some respects to those previously reported for glycine and L-alanine.

Introduction

In the last three decades vibrational spectroscopy has become an important technique for the structural characterization of peptides and proteins,[1] in particular, Raman and resonance Raman spectroscopy[2−4] and the chiroptical methods ROA[5] and VCD.[6] There have also been numerous vibrational studies of the constituent α-amino acids, although only limited attempts have been made to obtain detailed assignment of spectra through comparison with ab initio calculations. A major problem is that although α-amino acids exist in the zwitterionic state in neutral aqueous solutions and the solid state, they exist as neutral molecules in the gas phase. Consequently, ab initio calculations on isolated gas-phase molecules lead to the prediction of the neutral molecule as the species of lowest energy. There have been a number of calculations of the geometries and vibrational spectra of neutral forms of the two lowest molecular weight naturally occurring α-amino acids, glycine[7−12] and L-alanine,[13,14] including a recent DFT calculation of the neutral amino acids in the solid state.[15] Notwithstanding the quality of these studies, they are not relevant to glycine and L-alanine in terms of the occurrence of these amino acids in either the solid state or aqueous solution.

Treatment of biological molecules in the molecular/ionization forms that they take in aqueous solution is of fundamental importance since the vast majority of biochemical processes occur in an aqueous environment. Although zwitterionic α-amino acids can be modeled using the Hartree−Fock SCF method, such calculations lead to a poor prediction of molecular geometries and vibrational spectra owing to the lack of consideration of electron correlation. In the last 10 years hybrid SCF-DFT methods have become very popular because they treat electron correlation without a significant increase in computational resources and provide satisfactory predictions of structures and spectra. Unfortunately, all attempts using such methods to optimize α-amino acid zwitterion geometries result in proton transfer from the NH_3^+ group to the CO_2^- group, i.e., leading to the neutral species. This problem can be tackled in two ways: first, using a model representing a gas-phase cluster of an α-amino acid molecule with one or more hydrogen-bonded water molecules and, second, using self-consistent reaction field (SCRF) solvation methods to optimize the geometry of the zwitterion either in isolation or with hydrogen-bonded water molecules.

Although SCRF methods are computationally more demanding than calculations of isolated gas-phase molecules, inclusion of interaction with a solvent of high dielectric constant such as water leads to prediction of a stable zwitterionic species, even in the absence of explicit hydrogen-bonded water molecules. Nevertheless, the calculated geometries are not entirely satisfactory when compared with experimental data, often leading to a short distance between an ammonium ion proton and a carboxylate oxygen atom. For example, Gontrani et al.[16] and Tortonda et al.[17] carried out DFT calculations of glycine and L-alanine zwitterions using polarizable continuum models (PCM). In their optimized geometries the shortest distance between a NH_3^+ hydrogen atom and a CO_2^- oxygen atom was in the range 1.8−2 Å, i.e., within hydrogen-bonding distance. These results do not compare favorably with the published crystal structures of glycine[18] and L-alanine,[19] where the shortest H—O distance, around 2.5 Å, is too large for there to be any significant hydrogen bonding. Nóbrega et al.[20] performed DFT calculations of the L-alanine zwitterion using the Onsager dipole solvation method for solvents other than water. Their results predicted an H—O distance of around 2.1 Å in acetonitrile and ethanol, but in tetrachloromethane geometry optimization lead

* To whom correspondence should be addressed. E-mail: t.j.dines@dundee.ac.uk.
† University of Greenwich at Medway.
‡ University of Dundee.
§ Brunel University.

10.1021/jp8037945 CCC: $40.75
Published on Web 09/25/2008

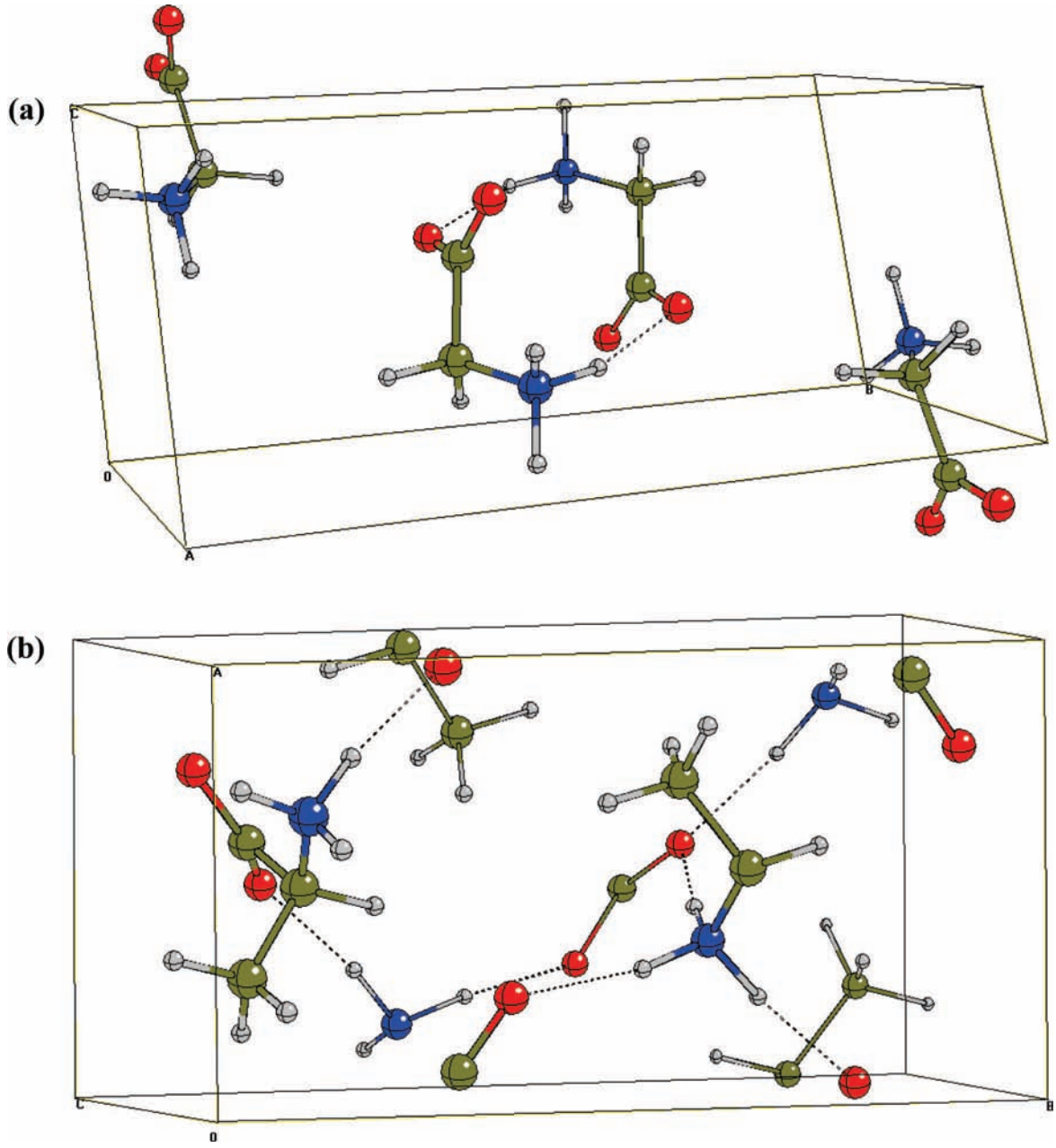

Figure 1. Optimized unit cell geometries (PW91 functional) for (a) glycine and (b) L-alanine.

to the neutral species (N—H = 1.871 Å). However, a recent DFT calculation of the structure of L-alanine in the solid state[21] is in good agreement with the crystal structure.

There have been several reports in the literature of quantum-chemical studies of gas-phase clusters of the zwitterions of glycine[22−29] and L-alanine[29−31] with one or more hydrogen-bonded water molecules. Thus, the effects of solvation are treated explicitly with specific solute−solvent interactions. Other computational studies of glycine[32] and L-alanine[33−36] zwitterions have included models incorporating hydrogen-bonded water molecules and made use of an SCRF method, usually either the Onsager dipole or PCM method. Comparison of the models employed reveals that none are able to accurately reproduce all features of the molecular geometries, and there appears to be no general agreement concerning how many hydrogen-bonded water molecules are actually required to produce a realistic structural model, although it is clear that a minimum of two water molecules are necessary to stabilize the zwitterions.

We further developed such a protocol for the accurate prediction of the structures and also the vibrational spectra of α-amino acids as part of an extensive program of DFT studies of amino acids and small peptides. This procedure has been applied to several of the essential α-amino acids, but in the present report we restrict the discussion to the two lowest molecular weight cases, glycine and L-alanine. Calculations were carried out on clusters of glycine and L-alanine zwitterions interacting with five hydrogen-bonded water molecules, such that all three ammonium ion protons are hydrogen bonded to water oxygen atoms and both carboxylate oxygen atoms are hydrogen bonded to water hydrogen atoms, in contrast to all previously reported models. These calculations were then repeated using the poarizable continuum model (PCM), which was shown to give a more satisfactory prediction of vibrational spectra. The structures and vibrational spectra of glycine and L-alanine in the solid state were also modeled using DFT calculations.

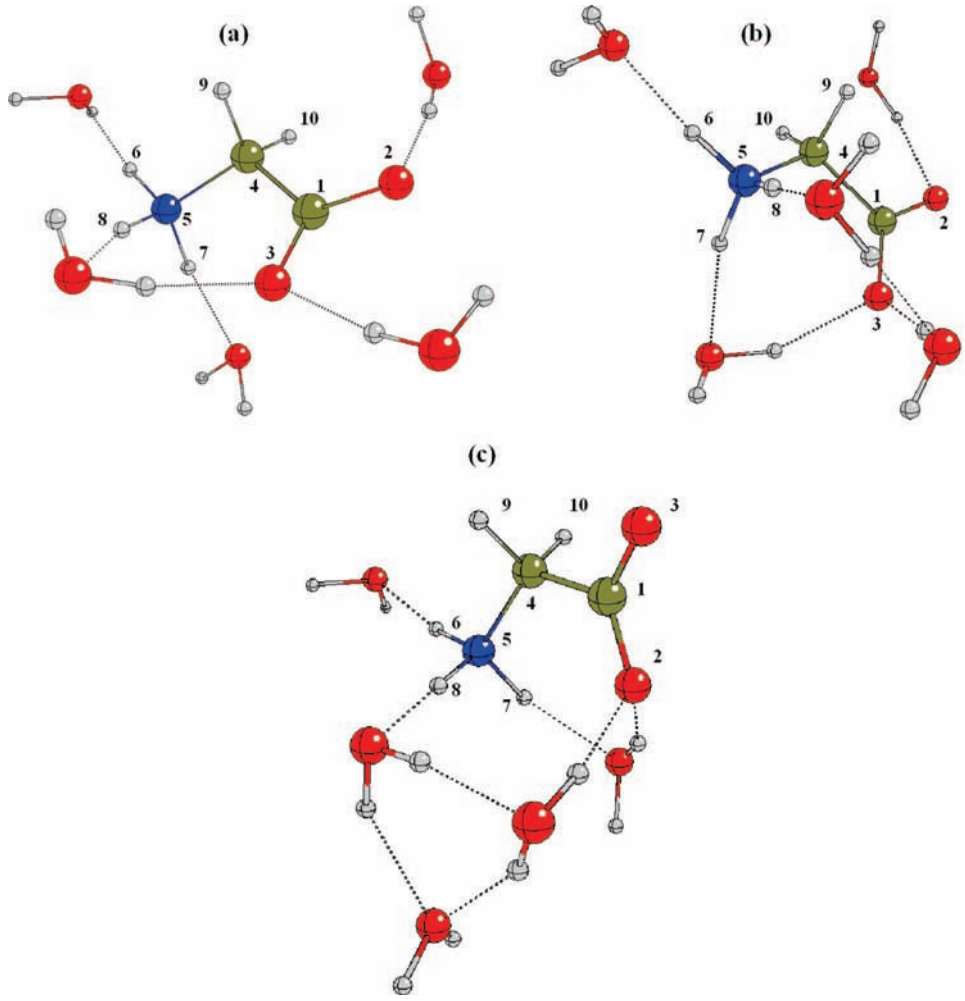

Figure 2. Calculated (B3-LYP/cc-pVDZ/IEF-PCM) structures of glycine-$(H_2O)_5$: (a) model I, (b) model II, and (c) model III.

TABLE 1: Comparison of Experimental and Calculated Unit Cell Dimensions[a]

(a) glycine [space group $P_{2_1/n}$ (C_{2h}^5)]	expt[18]	PW91	PBE
a	5.1054	5.2009	5.2021
b	11.968	12.7802	12.7815
c	5.4645	5.4600	5.4611
α	90.0	90.0	90.0
β	111.697	109.113	109.1018
γ	90.0	90.0	90.0
(b) L-alanine [space group P_{212121} (D_2^4)]	expt[19]	PW91	PBE
a	6.025	6.3376	6.4171
b	2.324	12.0897	12.1650
c	5.783	5.9037	5.8663
α	90.0	90.0	90.0
β	90.0	90.0	90.0
γ	90.0	90.0	90.0

[a] Distances are in Angstroms and angles in degrees.

Recently, Degtyarenko et al.[37,38] simulated the L-alanine zwitterion in aqueous solution using a Born−Oppenheimer molecular dynamics method. In this approach the L-alanine zwitterion with 50 water molecules was treated by DFT employing a double-ζ basis set with polarization functions for valence electrons and norm-conserving pseudopotentials for core electrons. Their results are especially significant in that they showed that at ambient temperature the carboxylate group exhibits no conformational preference but the methyl and ammonium groups prefer to remain in an almost staggered conformation with respect to the α H atom and eclipsed with respect to each other. In a subsequent study[39] they used the results of the molecular dynamics simulation to provide initial guesses for the positions of 20 water molecules in the first solvation shell of the solvated L-alanine zwitterion. The geometry of this cluster was optimized using DFT employing various continuum solvation methods from which vibrational spectra were computed. Their results are compared with those obtained in the present work.

Experimental Section

Glycine (Aldrich, Reagentplus grade, ≥ 99%) and L-alanine (Aldrich, 99%) were used without further purification. Raman spectra were recorded using a LabRam Raman spectrometer (ISA, Ltd.). The spectrometer is equipped with a 1800 line mm^{-1} holographic grating blazed at 500 nm, a holographic notch filter, a Peltier-cooled CCD (MPP1 chip) for detection, and an Olympus BX40 microscope. Samples were excited at 632.8 nm by a helium−neon laser with 8 mW power at the sample. Raman spectra of solid-state samples were collected at room temperature on a microscope slide using a ×50 microscope objective to focus the laser beam. Aqueous solution-phase spectra were acquired, at room temperature, using 1 cm path length quartz cuvettes and a concentration of 50 mg/mL for both amino acids. The Raman instrument was calibrated using the ν_1 line of silicon at 520.7 cm^{-1}. The centring of the silicon line and wavenumber

TABLE 2: Comparison of Experimental and Calculated Molecular Geometries of Glycine[a]

		solid DFT		B3-LYP/cc-pVDZ	
	expt[18]	PW91	PBE	gas	IEF-PCM
r(C1O2)	1.2527	1.2631	1.2644	1.2572	1.2545
r(C1O3)	1.2536	1.2692	1.2697	1.2637	1.2697
r(C1C4)	1.5262	1.5413	1.5414	1.5495	1.5418
r(C4N5)	1.4778	1.4876	1.4863	1.5044	1.4847
r(C4H9)	0.9628	1.0937	1.0958	1.0974	1.1027
r(C4H10)	0.9660	1.0996	1.1007	1.0945	1.0981
r(N5H6)	0.9957	1.0663	1.0668	1.0445	1.0492
r(N5H7)	0.9585	1.0469	1.0481	1.0749	1.0494
r(N5H8)	0.9810	1.0378	1.0379	1.0339	1.0486
r(O2···H)	1.7913	1.6576	1.6572	1.6946	1.7850
r(O3···H)	1.8808, 2.1802	1.7946, 1.9321	1.7950,1.9323	1.6706, 1.9704	1.7511, 1.8360
r(H6···O)	1.7913	1.6576	1.6572	1.7981	1.7422
r(H7···O)	2.1802	1.7946	1.7950	1.6350	1.7402
r(H8···O)	1.8808	1.9321	1.9323	1.9411	1.7669
θ(O2C1O3)	125.58	125.78	125.77	127.07	125.97
θ(O2C1C4)	117.46	116.61	116.63	116.36	116.04
θ(O3C1C4)	116.95	117.60	117.60	116.30	117.98
θ(C1C4N5)	111.70	111.96	112.00	107.24	113.46
θ(C1C4H9)	107.50	110.79	110.77	112.10	108.34
θ(C1C4H10)	112.26	109.39	109.33	110.66	109.19
θ(N5C4H9)	110.51	108.00	108.06	108.45	108.24
θ(N5C4H10)	106.12	108.58	108.65	107.59	109.85
θ(C4N5H6)	110.66	110.14	110.18	110.00	110.31
θ(C4N5H7)	110.12	112.68	112.67	109.68	110.02
θ(C4N5H8)	113.86	109.15	109.19	109.02	110.41
θ(H9C4H10)	108.78	108.02	107.93	110.61	107.58
θ(H6N5H7)	107.87	109.76	109.68	105.22	109.26
θ(H6N5H8)	107.27	107.71	107.72	116.51	109.04
θ(H7N5H8)	106.81	107.24	107.24	106.16	107.74
τ(O2C1C4N5)	−19.10	31.92	31.89	91.23	159.52
τ(O2C1C4H9)	102.27	152.56	152.61	−149.84	−80.26
τ(O2C1C4H10)	−138.17	−88.48	−88.59	−25.85	36.63
τ(O3C1C4N5)	161.83	−148.81	−148.77	−83.21	−21.68
τ(O3C1C4H9)	−76.81	−28.18	−28.05	35.71	98.55
τ(O3C1C4H10)	42.76	90.78	90.75	159.7	−144.56
τ(C1C4N5H6)	−178.46	174.21	174.27	−141.00	178.95
τ(C1C4N5H7)	−59.29	−62.87	−62.89	−25.82	−60.43
τ(C1C4N5H8)	60.63	56.15	56.15	90.03	58.36
τ(H6N5C4H9)	61.96	51.96	51.99	97.67	58.67
τ(H7N5C4H9)	−178.87	174.88	174.83	−147.04	179.29
τ(H8N5C4H9)	−58.95	−66.10	−66.12	−31.22	−61.92
τ(H6N5C4H10)	−55.81	−64.92	−64.86	−22.00	−58.53
τ(H7N5C4H10)	63.36	58.00	57.98	93.26	62.09
τ(H8N5C4H10)	−176.72	177.02	177.03	−150.83	−179.12

[a] Bond distances are in Angstroms and interbond angles and dihedral angles in degrees.

calibration was checked using the frequencies of the principal lines of a neon lamp.

IR spectra were recorded using a Perkin-Elmer Paragon 1000 FTIR instrument operating at a resolution of 1 cm^{-1} in the 450−4000 cm^{-1} range. A dry nitrogen gas purge was maintained in the sample compartment to facilitate a simpler background subtraction. Powdered (solid-state) samples were examined as pressed KBr discs.

Computational Details

SCF-DFT calculations of model structures of clusters of glycine and L-alanine molecules with hydrogen-bonded water molecules were carried out using the Gaussian03 program,[40] employing the hybrid SCF-density functional method B3-LYP.[41,42] In contrast to previously published DFT studies of α-amino acids, which all employed Pople-style split-valence basis sets, we used Dunning's correlation-consistent cc-pVDZ basis set,[43] which is of sufficient quality to yield satisfactory geometries and vibrational spectra. Furthermore, Dunning basis functions contain primitive Gaussian functions with small zeta values, such that additional diffuse functions are not usually needed for anions and atoms with lone pairs. The effect of solvation was investigated using the integral equation formalism polarizable continuum model (IEF-PCM).[44] The molecular cavity was defined using the united atom topological model,[45] i.e., by putting a sphere around each solute heavy atom with hydrogen atoms enclosed in the sphere of the heavy atom to which they are bonded.

DFT calculations of glycine and L-alanine in the solid state were carried using the plane-wave-pseudopotential CASTEP v4.2 program,[46] employing the generalized gradient approximation (GGA) functionals PW91[47] and PBE.[48] We used norm-conserving pseudopotentials optimized for GGA DFT methods with a basis set cut off energy of 816 eV. Brillouin zone integrations were performed with a 2,2,2 Monkhorst-Pack[49] grid, and the Broyden−Fletcher−Goldfarb−Shanno optimization scheme was used. Lattice parameters and atomic positions were optimized according to the following criteria: total energy

TABLE 3: Comparison of Experimental and Calculated Molecular Geometries of L-Alanine[a]

		solid DFT		B3-LYP/cc-pVDZ	
	expt[19]	PW91	PBE	gas	IEF-PCM
r(C1O2)	1.2399	1.2546	1.2560	1.2408	1.2549
r(C1O3)	1.2569	1.2770	1.2767	1.2811	1.2704
r(C1C4)	1.5305	1.5497	1.5504	1.5576	1.5484
r(C4N5)	1.4859	1.4955	1.4942	1.5028	1.4942
r(C4C9)	1.5221	1.5323	1.5329	1.5288	1.5303
r(C4H10)	1.0913	1.0981	1.0994	1.1004	1.0995
r(N5H6)	1.0469	1.0608	1.0586	1.0351	1.0469
r(N5H7)	1.0297	1.0435	1.0442	1.0522	1.0489
r(N5H8)	1.0275	1.0399	1.0396	1.0495	1.0486
r(C9H11)	1.0800	1.0954	1.0971	1.1023	1.1006
r(C9H12)	1.0815	1.0947	1.0961	1.0967	1.0990
r(C9H13)	1.0797	1.0967	1.0984	1.1021	1.1025
r(O2···H)	1.861	1.8499	1.8678	1.8087	1.7850
r(O3···H)	1.780, 1.828	1.7303, 1.8450	1.7518, 1.8478	1.7424, 1.8140	1.7585, 1.8371
r(H6···O)	1.861	1.8499	1.8678	1.8599	1.7673
r(H7···O)	1.780	1.7303	1.7518	1.7455	1.7404
r(H8···O)	1.828	1.8450	1.8478	1.7500	1.7706
θ(O2C1O3)	125.62	126.00	125.82	126.95	125.77
θ(O2C1C4)	118.36	118.38	118.32	115.86	116.12
θ(O3C1C4)	116.02	115.62	115.86	117.19	118.08
θ(C1C4N5)	110.13	110.82	110.75	111.08	111.53
θ(C1C4C9)	111.09	110.68	111.34	111.99	110.99
θ(C1C4H10)	108.55	108.40	108.48	107.54	107.66
θ(N5C4C9)	109.75	109.60	109.67	109.60	109.67
θ(N5C4H10)	106.88	106.87	106.70	107.37	107.59
θ(C4N5H6)	109.44	109.97	109.37	109.76	109.58
θ(C4N5H7)	109.02	109.85	110.43	111.33	110.36
θ(C4N5H8)	111.25	111.27	111.35	108.88	110.34
θ(C9C4H10)	110.35	110.40	109.78	109.12	109.30
θ(C4C9H11)	110.38	110.41	110.34	110.23	110.28
θ(C4C9H12)	110.57	110.95	110.21	108.14	109.32
θ(C4C9H13)	110.24	110.48	110.79	110.99	110.74
θ(H6N5H7)	108.20	108.73	108.22	111.00	109.63
θ(H6N5H8)	108.19	107.37	107.91	110.66	109.05
θ(H7N5H8)	110.69	109.59	109.48	105.10	107.84
θ(H11C9H12)	108.98	107.97	108.30	108.38	109.04
θ(H11C9H13)	108.36	108.59	108.63	108.78	108.76
θ(H12C9H13)	108.26	108.37	108.50	110.28	108.66
τ(O2C1C4N5)	−18.63	−20.81	−20.80	173.14	158.11
τ(O2C1C4C9)	103.18	101.00	101.51	−63.95	−79.28
τ(O2C1C4H10)	−135.33	−137.79	−137.59	55.92	40.30
τ(O3C1C4N5)	161.44	159.90	159.57	−7.31	−23.45
τ(O3C1C4C9)	−76.76	−78.30	−78.11	115.60	99.15
τ(O3C1C4H10)	44.74	42.91	42.79	−124.53	−141.26
τ(C1C4N5H6)	177.83	176.66	178.91	−174.35	−179.20
τ(C1C4N5H7)	−64.01	−63.71	−62.11	−51.05	−5 8.38
τ(C1C4N5H8)	58.33	57.82	59.74	64.37	60.71
τ(C1C4C9H11)	175.91	178.00	175.77	−176.30	179.28
τ(C1C4C9H12)	55.25	58.34	56.22	65.38	59.40
τ(C1C4C9H13)	−64.42	−61.87	−63.88	−55.71	− 60.30
τ(H6N5C4C9)	55.24	54.22	55.63	61.37	57.44
τ(H7N5C4C9)	173.4	173.85	174.61	−175.32	178.25
τ(H8N5C4C9)	−64.26	−64.62	−63.55	−59.91	−6 2.66
τ(N5C4C9H11)	−62.07	−59.48	−61.29	−52.55	− 57.04
τ(N5C4C9H12)	177.27	−179.14	179.15	−170.88	−176.92
τ(N5C4C9H13)	57.6	60.65	59.05	68.04	63.38
τ(H6N5C4H10)	−64.43	−65.43	−63.21	−57.03	− 61.35
τ(H7N5C4H10)	53.72	54.20	55.77	66.28	59.47
τ(H8N5C4H10	176.07	175.73	177.62	−178.30	178.55
τ(H11C9C4H10)	55.47	57.98	55.63	64.75	60.68
τ(H12C9C4H10)	−65.19	−61.68	−63.93	−53.57	−59.19
τ(H13C9C4H10)	175.14	178.11	175.97	−174.66	−178.89

[a] Bond distances are in Angstroms and interbond angles and dihedral angles in degrees.

convergence $< 2 \times 10^{-5}$ eV/atom, maximum force on any atom < 0.05 eV/Å, stress < 0.1 GPa, and atomic displacements $< 10^{-3}$ Å.

For the model zwitterion−water clusters force constants dipole derivatives and polarizability derivatives were calculated at the optimized geometry using the same DFT method and basis

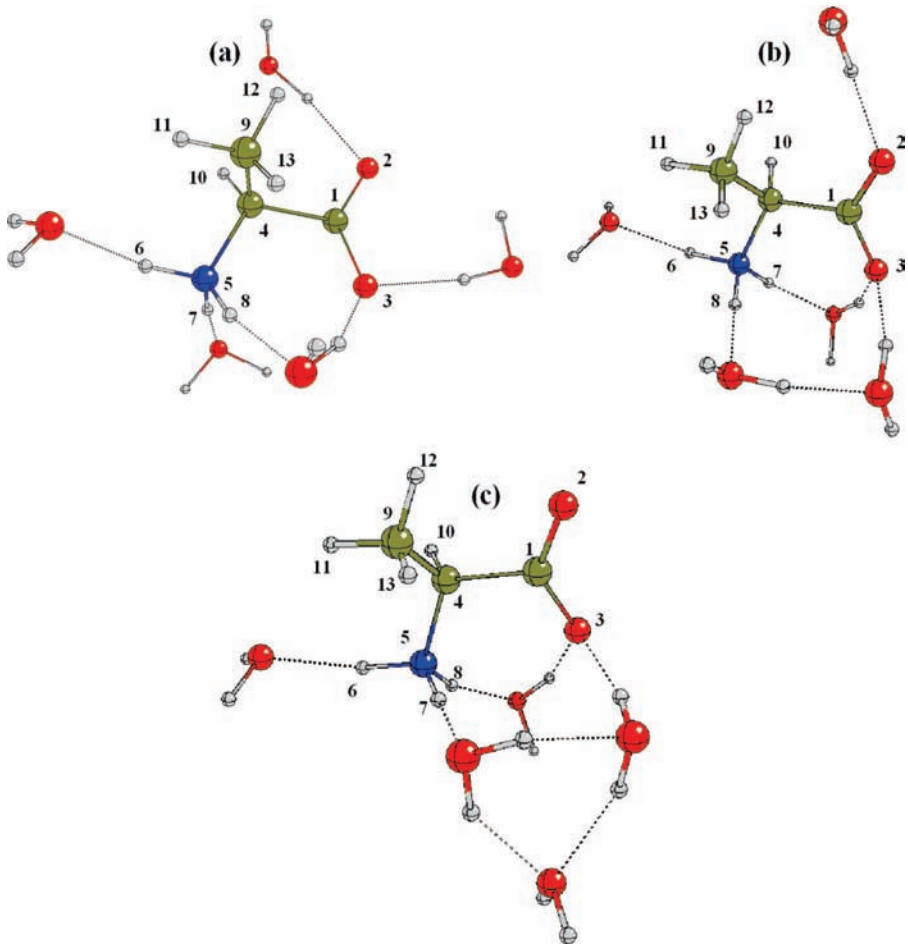

Figure 3. Calculated (B3-LYP/cc-pVDZ/IEF-PCM) structures of L-alanine-$(H_2O)_5$: (a) model I, (b) model II, and (c) model III.

TABLE 4: Computed Energies from the B3-LYP/cc-pVDZ/IEF-PCM Calculations of α-Amino Acid−Water Model Clusters

	model	*E*/H	Δ*E*/kJ mol^{-1}
glycine−$(H_2O)_5$	I	−666.689535787	0
	II	−666.698074956	−22.42
	III	−666.697446994	−20.77
alanine−$(H_2O)_5$	I	−706.008149130	0
	II	−706.017911067	−25.63
	III	−706.016252824	−21.28

set with and without the IEF-PCM method. In order to compute the potential-energy distributions associated with each vibrational mode the Cartesian force constants obtained from the Gaussian03 output were converted to general valence force field (GVFF) force constants, expressed in terms of internal coordinates, and scaled before input to a normal coordinate analysis program derived from those of Schachtschneider.[50] At this stage, the force constants, dipole derivatives, and polarizability derivatives associated with hydrogen-bonded water molecules were removed. Scaling of force constants, expressed in internal coordinates, was applied according to the following formula

$$f_{ij}^{\text{scaled}} = f_{if}^{\text{calcd}} \sqrt{s_i s_j}$$

where s_i and s_j are scale factors relating to internal coordinates i and j following the Pulay SQM-FF method.[51] For comparison with experimental spectra, simulated IR and Raman spectra were obtained by convolution of computed band intensities with a Lorentzian line shape function (fwhm = 10 cm^{-1}).

DFT calculations of the vibrational spectra of glycine and L-alanine in the solid state were carried out at their optimized geometries at the gamma-point only, and assignments were determined by visualization of the phonon eigenvectors using the Moldraw program.[52] Simulated IR spectra were obtained by convolution of computed band intensities with a Lorentzian line shape function (fwhm = 10 cm^{-1}). Raman intensities are not provided by CASTEP, and experimental Raman spectra were compared only with tabulated computed Raman band positions.

Results and Discussion

Geometry. The published crystal structures of glycine[18] and L-alanine[19] at room temperature were used as starting points for geometry optimization in both the solution-phase model and solid-state calculations. For both amino acids there are four molecules per unit cell but the space groups are different, i.e., $P_{2_1/n}$ for glycine and P_{212121} for L-alanine. Optimized unit cell geometries are shown in Figure 1, unit cell parameters are listed in Table 1, and the calculated bond distances, interbond angles, and dihedral angles are listed in Tables 2 and 3. For the geometry optimization in the solid state the unit cell symmetry was constrained, and this proved to be justifiable in that the phonon calculation for glycine (vide infra) yielded no imaginary frequencies other than those for acoustic modes and for L-alanine gave only 1 imaginary frequency in addition to those for the acoustic modes. The computed geometries compare favorably with those reported in recent DFT studies of glycine[50] and L-alanine.[21]

Aqueous solution-phase models for glycine and L-alanine zwitterions were initially treated as gas-phase clusters in

TABLE 5: Scale Factors and Scaled GVFF Principal Force Constants (mdyn Å^{-1}) for Model I Structures

r(CH)	0.90	*θ*(XCH)	0.95	
r(NH)	0.99	*θ*(XNH)	0.95	(X = N, C, or H)
others	0.98			

	glycine		L-alanine	
internal coordinate	gas-phase	IEF-PCM	gas-phase	IEF-PCM
r(N5H6)	5.499	5.157	6.033	5.297
r(N5H7)	3.931	5.170	5.032	5.158
r(N5H8)	6.144	5.181	5.216	5.207
r(C4 × 9)	4.830	4.661	4.320	4.401
r(C4H10)	4.937	4.826	4.740	4.740
r(C9H11)			4.707	4.771
r(C9H12)			4.917	4.821
r(C9H13)			4.713	4.705
r(C1O2)	10.000	9.848	10.891	9.791
r(C1O3)	9.676	9.082	8.618	9.037
r(C1C4)	3.833	4.093	3.834	4.059
r(C4N5)	4.597	4.877	4.442	4.585
θ(C4N5H6)	0.548	0.549	0.503	0.552
θ(C4N5H7)	0.732	0.571	0.598	0.574
θ(C4N5H8)	0.494	0.565	0.574	0.567
θ(H7N5H8)	0.243	0.244	0.244	0.245
θ(H6N5H7)	0.249	0.245	0.246	0.243
θ(H6N5H8)	0.226	0.245	0.234	0.242
θ(C4C9H11)			0.467	0.453
θ(C4C9H12)			0.450	0.424
θ(C4C9H13)			0.455	0.448
θ(H12C9H13)			0.203	0.202
θ(H11C9H12)			0.201	0.202
θ(H11C9H13)			0.215	0.212
θ(X9C4H10)	0.094	0.092	0.138	0.128
θ(C1C4N5)	0.895	0.979	0.505	0.419
θ(C1C4 × 9)	0.203	0.215	0.372	0.288
θ(C1C4H10)	0.200	0.275	0.107	0.113
θ(N5C4 × 9)	0.284	0.290	0.441	0.437
θ(N5C4H10)	0.297	0.294	0.128	0.121
θ(O2C1O3)	0.980	0.991	0.983	1.002
θ(O2C1C4)	0.873	0.856	0.894	0.878
θ(O3C1C4)	0.874	0.965	0.963	0.982
ω(CO_2)	0.093	0.081	0.090	0.082
τ(C1C4)	0.098 ± 0.013	0.081 ± 0.004	0.091 ± 0.022	0.082 ± 0.018
τ(C4N5)	0.074 ± 0.010	0.072 ± 0.004	0.077 ± 0.012	0.074 ± 0.009
τ(C4C9)			0.083 ± 0.021	0.079 ± 0.017

which a water molecule was placed in close proximity (1.8 Å) to each of the five possible hydrogen-bonding sites, i.e., each ammonium ion hydrogen atom and each carboxylate oxygen atom. The molecular geometry of the gas-phase cluster model for each amino acid was optimized at the B3-LYP/cc-pVDZ level (details in Tables 2 and 3). Since we are not concerned in this study with the energies associated with hydrogen bonding, no correction was made for basis set superposition error. Although the isolated glycine molecule has a plane of symmetry (C_s point group) this symmetry cannot be retained in the glycine−water cluster without imposing severe restraints on the structure, leading to an inappropriate optimized geometry.

The optimized structure of the gas-phase model for each amino acid was used as the initial geometry for SCRF calculations involving the IEF-PCM method with water as solvent ($\epsilon_r = 78.39$) and the molecular cavity defined by the united atom topological model. This optimized geometry is referred to as model I. Two additional model clusters of each amino acid with five water hydrogen-bonded molecules were also investigated using the IEF-PCM method. In these the initial guesses for the molecular geometries involved (i) two water molecules bridging between the ammonium and carboxylate groups (model II) and (ii) three water molecules bridging between the ammonium and carboxylate groups (model III). The optimized geometries for all three models together with the atom-numbering schemes are shown in Figure 2 for glycine and Figure 3 for L-alanine. Computed bond distances, interbond angles, and dihedral angles for model I only are listed in Tables 2 and 3, and the corresponding data for models II and III are provided in Tables S1 and S2 in the Supporting Information.

Computed energies for the three models are listed in Table 4. Although models II and III are energetically more favorable than model I by ca. 20−25 kJ mol^{-1}, for both glycine and L-alanine we consider these to be less satisfactory models, especially because there is a greater difference between the two CO bond distances than for model I. This is reflected in a greater difference between the wavenumbers of bands attributed to ν_{as}(CO) and ν_s(CO) motions (vide infra). Although 20 kJ mol^{-1} is significantly greater than kT at room temperature (2.48 kJ mol^{-1}) we believe model I provides a more realistic "average" amino acid geometry, as evidenced by the vibrational spectra in aqueous solution.

In order to check that the zwitterion is more stable than the neutral species for these solvated clusters we also carried out a calculation on the neutral species of glycine with five hydrogen-bonded water molecules using the same method and basis set. The initial geometry for this calculation was derived from model I with the hydrogen atom labeled H8 transferred to the oxygen atom O3 with the H_2O positions unchanged. Geometry optimization resulted in a structure in

TABLE 6: Definitions of Internal Coordinates Adapted to Local Symmetry[a]

(a) glycine

$\nu_s(NH_3) = 1/\sqrt{3}[r(N5H6) + r(N5H7) + r(N5H8)]$
$\nu_{as}(NH_3) = 1/\sqrt{6}[2r(N5H6) - r(N5H7) - r(N5H8)]$
$\nu_{as'}(NH_3) = 1/\sqrt{2}[r(N5H7) - r(N5H8)]$
$\nu_s(CH_2) = 1/\sqrt{2}\ [r(C4H9) + r(C4H10)]$
$\nu_{as}(CH_2) = 1/\sqrt{2}\ [r(C4H9) - r(C4H10)]$
$\nu_s(CO_2) = 1/\sqrt{2}\ [r(C1O2) + r(C1O3)]$
$\nu_{as}(CO_2) = 1/\sqrt{2}\ [r(C1O2) - r(C1O3)]$
$\nu(CC) = r(C1C4)$
$\nu(CN) = r(C4N5)$
$\delta_s(NH_3) = 1/\sqrt{6}[\theta(C4N5H6) + \theta(C4N5H7) + \theta(C4N5H8) - \theta(H7N5H8) - \theta(C6N5H7) - \theta(H6N5H8)]$
$\delta_{as}(NH_3) = 1/\sqrt{6}[2\theta(H7N5H8)\text{-}\theta(C6N5H7)\text{-}\theta(H6N5H8)]$
$\delta_{as'}(NH_3) = 1/\sqrt{2}[\theta(C6N5H7) - \theta(H6N5H8)]$
$\rho_{ip}(NH_3) = 1/\sqrt{6}[2\theta(C4N5H6) - \theta(C4N5H7) - \theta(C4N5H8)]$
$\rho_{op}(NH_3) = 1/\sqrt{2}[\theta(C4N5H7) - \theta(C4N5H8)]$
$\delta(CH_2) = 1/2\sqrt{6}[(2 + \sqrt{6})\theta(H9C4H10) + (2 - \sqrt{6})\theta(C1C4N5) - \theta(C1C4H9) - \theta(C1C4H10) - \theta(N5C4H9) - \theta(N5C4H10)]$
$\delta(CCN) = 1/2\sqrt{6}[(2 - \sqrt{6})\theta(H9C4H10) + (2 + \sqrt{6})\theta(C1C4N5) - \theta(C1C4H9) - \theta(C1C4H10) - \theta(N5C4H9) - \theta(N5C4H10)]$
$\rho(CH_2) = 1/2[\theta(C1C4H9)\text{-}\ \theta(C1C4H10) + \theta(N5C4H9)\text{-}\ \theta(N5C4H10)]$
$\omega(CH_2) = 1/2[\theta(C1C4H9) + \theta(C1C4H10) - \theta(N5C4H9) - \theta(N5C4H10)]$
$\tau(CH_2) = 1/2[\theta(C1C4H9) - \theta(C1C4H10) - \theta(N5C4H9) + \theta(N5C4H10)]$
$\delta(CO_2) = 1/\sqrt{6}[2\theta(O2C1O3) - \theta(O2C1C4) - \theta(O3C1C4)]$
$\rho(CO_2) = 1/\sqrt{2}[\theta(O2C1C4) - \theta(O3C1C4)]$
$\omega(CO_2) = 1/\sqrt{2}[\phi(C1O2) + \phi(C1O3)]$
$\tau(CC) = 1/\sqrt{6}[\tau(O2C1C4N5) + \tau(O2C1C4H9) + \tau(O2C1C4H10) + \tau(O3C1C4N5) + \tau(O3C1C4H9) + \tau(O3C1C4H10)]$
$\tau(CN) = 1/3[\tau(C1C4N5H6) + \tau(C1C4N5H7) + \tau(C1C4N5H8) + \tau(H9C4N5H6) + \tau(H9C4N5H7) + \tau(H9C4N5H8) + \tau(H10C4N5H6) + \tau(H10C4N5H7) + \tau(H10C4N5H8)]$

(b) L-alanine

$\nu_s(NH_3) = 1/\sqrt{3}[r(N5H6) + r(N5H7) + r(N5H8)]$
$\nu_{as}(NH_3) = 1/\sqrt{6}[2r(N5H6) - r(N5H7) - r(N5H8)]$
$\nu_{as'}(NH_3) = 1/\sqrt{2}[r(N5H7) - r(N5H8)]$
$\nu(CH) = \nu(C4H10)$
$\nu_s(CH_3) = 1/\sqrt{3}[r(C9H11) + r(C9H12) + r(C9H13)]$
$\nu_{as}(CH_3) = 1/\sqrt{6}[2r(C9H11) - r(C9H12) - r(C9H13)]$
$\nu_{as'}(CH_3) = 1/\sqrt{2}[r(C9H12) - r(C9H13)]$
$\nu_s(CO_2) = 1/\sqrt{2}[r(C1O2) + r(C1O3)]$
$\nu_{as}(CO_2) = 1/\sqrt{2}[r(C1O2) - r(C1O3)]$
$\nu(C1C4) = r(C1C4)$
$\nu(C4C9) = r(C4C9)$
$\nu(CN) = r(C4N5)$
$\delta_s(NH_3) = 1/\sqrt{6}[\theta(C4N5H6) + \theta(C4N5H7) + \theta(C4N5H8) - \theta(H7N5H8) - \theta(C6N5H7) - \theta(H6N5H8)]$
$\delta_{as}(NH_3) = 1/\sqrt{6}[2\theta(H7N5H8) - \theta(C6N5H7) - \theta(H6N5H8)]$
$\delta_{as'}(NH_3) = 1/\sqrt{2}[\theta(C6N5H7) - \theta(H6N5H8)]$
$\rho_{ip}(NH_3) = 1/\sqrt{6}[2\theta(C4N5H6) - \theta(C4N5H7) - \theta(C4N5H8)]$
$\rho_{op}(NH_3) = 1/\sqrt{2}[\theta(C4N5H7) - \theta(C4N5H8)]$
$\delta_s(CH_3) = 1/\sqrt{6}[\theta(C4C9H11) + \theta(C4C9H12) + \theta(C4C9H13) - \theta(H12C9H13) - \theta(H11C9H12) - \theta(H11C9H13)]$
$\delta_{as}(CH_3) = 1/\sqrt{6}[2\theta(H12C9H13) - \theta(H11C9H12) - \theta(H11C9H13)]$
$\delta_{as'}(CH_3) = 1/\sqrt{2}[\theta(H11C9H12) - \theta(H11C9H13)]$
$\rho_{ip}(CH_3) = 1/\sqrt{6}[2\theta(C4C9H11) - \theta(C4C9H12) - \theta(C4C9H13)]$
$\rho_{op}(CH_3) = 1/\sqrt{2}[\theta(C4C9H12) - \theta(C4C9H13)]$
$\rho(CH) = 1/\sqrt{6}[2\theta(N5C4H10) - \theta(C1C4H10) - \theta(C9C4H10)]$
$\rho'(CH) = 1/\sqrt{2}[\theta(C1C4H10) - \theta(C9C4H10)]$
$\delta(C1C4N) = \theta(C1C4N)$
$\delta(C9C4N) = \theta(C9C4N)$
$\delta(CCC) = \theta(C1C4C9)$
$\delta(CO_2) = 1/\sqrt{6}[2\theta(O2C1O3) - \theta(O2C1C4) - \theta(O3C1C4)]$
$\rho(CO_2) = 1/\sqrt{2}[\theta(O2C1C4) - \theta(O3C1C4)]$
$\omega(CO_2) = 1/\sqrt{2}[\phi(C1O2) + \phi(C1O3)]$
$\tau(C1C4) = 1/\sqrt{6}[\tau(O2C1C4N5) + \tau(O2C1C4H9) + \tau(O2C1C4H10) + \tau(O3C1C4N5) + \tau(O3C1C4H9) + \tau(O3C1C4H10)]$
$\tau(CN) = 1/3[\tau(C1C4N5H6) + \tau(C1C4N5H7) + \tau(C1C4N5H8) + \tau(C9C4N5H6) + \tau(C9C4N5H7) + \tau(C9C4N5H8) + \tau(H10C4N5H6) + \tau(H10C4N5H7) + \tau(H10C4N5H8)]$
$\tau(C4C9) = 1/3[\tau(C1C4C9H11) + \tau(C1C4C9H12) + \tau(C1C4C9H13) + \tau(N5C4C9H11) + \tau(N5C4C9H12) + \tau(N5C4C9H13) + \tau(H10C4C9H11) + \tau(H10C4C9H12) + \tau(H10C4C9H13)]$

[a] ϕ(C1O2) is the angle between the bond C1O2 and the plane containing atoms C1, O3, and C4. ϕ(C1O3) is the angle between the bond C1O3 and the plane containing atoms C1, O2, and C4.

which the H8 atom, though remaining bonded to O3, had moved to a position 1.662 Å from N5, thus representing an intermediate structure between the neutral species and zwitterion. The computed energy for this model was 48.6 kJ mol^{-1} higher than that of zwitterion model I. We can therefore be confident that in the presence of hydrogen-bonded water the zwitterion is significantly more stable than the neutral species, in agreement with overwhelming experimental evidence that only the zwitterion exists in aqueous solution.

The DFT calculations of glycine$-(H_2O)_5$ and L-alanine$-(H_2O)_5$ model I clusters generally agree well with solid-state

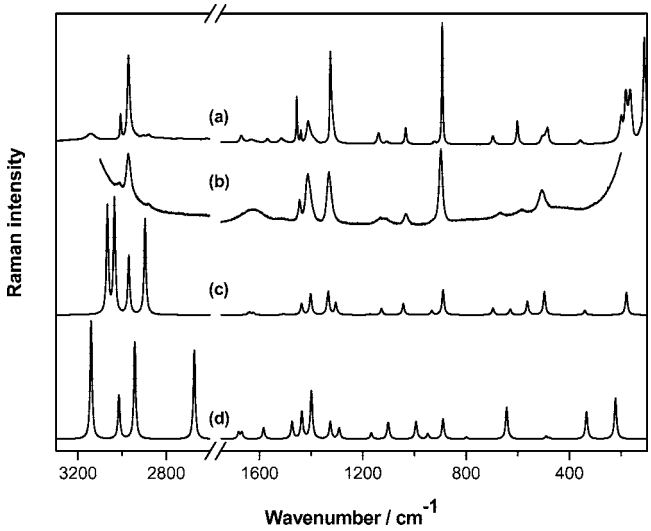

Figure 4. Raman spectrum of glycine in the solid state (a) and aqueous solution (b), and the simulated Raman spectra of the glycine model with five hydrogen-bonded water molecule models: IEF-PCM calculation (c) and gas-phase cluster calculation (d).

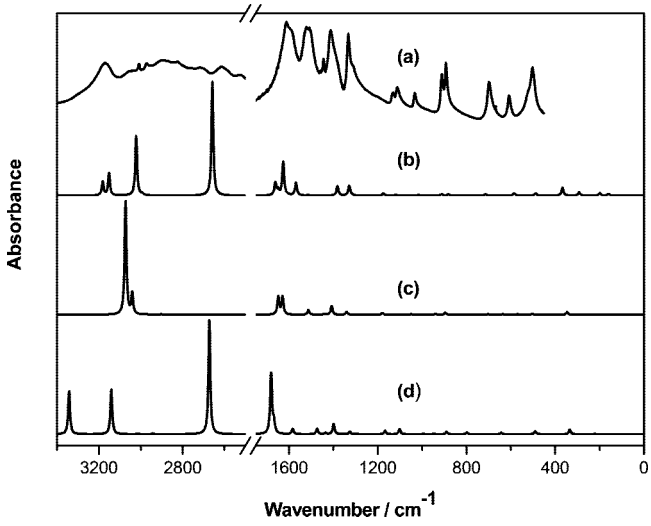

Figure 5. IR spectrum of glycine in the solid state (a), the simulated IR spectra of solid glycine (PW91 functional) (b), and the simulated IR spectra of the glycine model with five hydrogen-bonded water molecules models: IEF-PCM calculation (c) and gas-phase cluster calculation (d).

experimental geometries, although both the gas-phase and IEF-PCM calculations suggest a small difference between the two CO bond distances, whereas the experimental values are the same to within 0.036%. By contrast, the experimental CO distances are significantly different for L-alanine, reflecting stronger hydrogen bonding at O2, and this is accurately reproduced in the calculations, although the latter give CO distances which are about 1.5% longer than the experimental values. It is also noted that the gas-phase cluster calculation gives a large difference (0.04 Å) between *r*(C1O2) and *r*(C1O3).

Other computed bond distances are in reasonable agreement with experimental data for both amino acids. The experimental NH and CH distances for glycine appear to be unreasonably small, which we attribute to the difficulty in estimating hydrogen atom positions in X-ray crystallography. The bond distances obtained for both glycine and L-alanine using the IEF-PCM model are generally comparable with those of the isolated zwitterions reported by Gontrani et al.[16] in a B3-LYP/6-31G(d) PCM calculation and those of Tortonda et al.[17] in a B3-PW91/6-31+G(d,p) calculation using a continuum method. However, in both of those studies a short distance was computed between O2 and H8 (1.8−2.0 Å), indicating strong intramolecular hydrogen bonding in the absence of surrounding water molecules. This was reflected in our own SCRF calculations (Onsager and PCM models) of the isolated zwitterions (not reported), and it is clearly necessary to include explicit water molecules within the solvation model in order to obtain the correct zwitterion geometry. Derbel et al.[25] obtained a comparable geometry for the glycine zwitterion surrounded by 12 water molecules using a gas-phase B3-LYP/6-31++G(d) calculation. Thus, it appears that inclusion of a large number of water molecules in a gas-phase cluster model obviates the need for use of an implicit solvation model, but such a calculation is more computationally demanding.

Examination of computed interbond angles reveals no serious discrepancies with respect to solid-state experimental values although, not surprisingly, agreement is poorer for the aqueous solution models than for the solid-state DFT calculations. By contrast, there are some significant differences between computed and experimental dihedral angles. These differences are more marked for the aqueous solution models, especially with respect to the relative orientation of NH_3^+ and CO_2^- groups. This not surprising since it might reasonably be expected that dihedral angles in solution would differ on account of the influence of crystal packing forces in the solid state compared with less restricted internal rotation in aqueous solution. There are low-energy barriers for torsion about the CC and CN bonds of glycine and L-alanine in aqueous solution, and we therefore made no attempt to map the conformational landscapes of either molecule and simply sought the lowest energy-optimized structure in each case. It is important to note that the α-amino acid−water cluster is constantly evolving, as evidenced by the published MD simulations for L-alanine,[37,38] and that any computed model is only a "snapshot" view, which we consider to be acceptable provided it yields a satisfactory interpretation of vibrational spectra.

Force Constants. The vibrational spectra for the aqueous solution-phase models of glycine and L-alanine with five hydrogen-bonded water molecules were calculated at their optimized geometries using the B3-LYP/cc-pVDZ method for both the gas-phase cluster and IEF-PCM models. As previously noted, the force constants, dipole derivatives, and polarizability derivatives associated with hydrogen-bonded water molecules were removed, and the computed Cartesian force constants were scaled in order to match the experimental vibrational spectra. We sought to avoid the use of a large number of adjustable parameters and chose the scale factors listed in Table 5 together with the scaled GVFF principal force constants for model I. The scale factors provide a means of correcting for anharmonicity, and although a different set of values could have been chosen for each model we selected values which give the best fit for the IEF-PCM model I calculation. In order to facilitate comparison between the gas-phase and IEF-PCM models the same scale factors were used for both. For computation of vibrational spectra redundant internal coordinates were removed by taking appropriate linear combinations, adapted to local symmetry, in order to simplify the potential-energy distributions (p.e.d.s); the symmetry-adapted internal coordinates are listed in Table 6.

TABLE 7: Experimental (IR and Raman) Vibrational Spectra (cm^{-1}) of Glycine Compared with Scaled Calculated Values for the Glycine−Water Cluster

	Raman		B3LYP/cc-pVDZ		
IR solid	solid	soln	gas	IEF-PCM	assignments (% p.e.d.)
3160	3143		3342	3068	$\nu_{as'}(NH_3)$ (94)
			3141	3067	$\nu_{as}(NH_3)$ (96)
3006	3008	3013	2673	3035	$\nu_s(NH_3)$ (97)
2962	2972	2971	3014	2970	$\nu_s(CH_2)$ (16), $\nu_{as}(CH_2)$ (82)
2892			2943	2896	$\nu_s(CH_2)$ (83), $\nu_{as}(CH_2)$ (16)
1660sh	1671		1681	1642	$\nu_{as}(CO_2)$ (42), $\delta_{as}(NH_3)$ (28) $\delta_{as'}(NH_3)$ (18)
1609	1629		1668	1637	$\delta_{as}(NH_3)$ (42), $\delta_{as'}(NH_3)$ (45)
1589	1568		1583	1623	$\nu_{as}(CO_2)$ (44), $\delta_{as}(NH_3)$ (17) $\delta_{as'}(NH_3)$ (23)
1516, 1506	1515	1511	1473	1507	δ_s (NH_3) (94)
1444	1455	1445	1436	1437	$\nu_s(CO_2)$ (12), $\delta(CH_2)$ (72)
1411, 1385sh	1411, 1387	1412	1399	1402	ν_s (CO_2) (39), ν(CC) (13), $\delta(CH_2)$ (25)
1332	1325	1331	1326	1334	$\nu_s(CO_2)$ (24), $\omega(CH_2)$ (59)
1311sh	1312		1292	1304	$\rho_{op}(NH_3)$ (29), $\tau(CH_2)$ (54)
1129	1139	1130	1167	1173	$\rho_{ip}(NH_3)$ (67), $\omega(CH_2)$ (14)
1109	1108	1110	1102	1128	$\rho_{op}(NH_3)$ (42), $\tau(CH_2)$ (38)
1032	1034		994	1043	ν(CN) (80)
910	923		948	933	$\rho_{op}(NH_3)$ (17), $\rho(CH_2)$ (57), $\omega(CO_2)$ (21)
892	892	898	890	889	$\nu_s(CO_2)$ (20), ν(CC) (36), $\delta(CO_2)$ (28)
687	697	669	799	696	ν(CN) (10), δ(CCN) (15), $\delta(CO_2)$ (38), $\omega(CO_2)$ (17)
606	601	585	643	629	ν (CC) (12), $\delta(CO_2)$ (15), $\omega(CO_2)$ (31), τ(CN) (36)
	504sh	506	491	563	$\rho(CH_2)$ (12), $\omega(CO_2)$ (12), τ(CN) (53)
502	486		479	497	$\rho(CO_2)$ (50)
	359		334	341	δ(CCN) (60), $\omega(CO_2)$ (32)
	199				
	181				
	165		222	180	τ(CC) (100)

TABLE 8: Solid-State IR and Raman Spectra (cm^{-1}) of Glycine Compared with Calculated Values for Glycine in the Solid State Using the PW91 Functional

		calcd PW91				
IR solid	Raman solid	a_g	b_g	a_u	b_u	assignments
3160	3143	3128	3129	3152	3182	ν(N5H8)
3006	3008	2971	2971	2971	3022	ν(N5H7)
2962	2972	3074	3075	3075	3074	$\nu_{as}(CH_2)$
2892		2994	2996	2998	2994	$\nu_s(CH_2)$
		2649	2651	2657	2658	ν(N5H6)
1660sh	1671	1699	1701	1649	1649	$\delta_{as'}(NH_3)$
1609	1629	1660	1659	1657	1662	$\delta_{as}(NH_3)$
1589	1568	1521	1529	1597	1626	$\nu_{as}(CO_2)$; $\delta_s(NH_3)$
1516, 1506	1515	1566	1565	1513	1568	$\delta_s(NH_3)$; $\nu_{as}(CO_2)$
1444	1455	1433	1449	1452	1435	$\delta(CH_2)$
1411, 1385sh	1411, 1387	1380	1382	1382	1382	$\nu_s(CO_2)$; ν(CC); $\omega(CH_2)$; $\rho_{op}(NH_3)$
1332	1325	1324	1327	1327	1329	$\nu_s(CO_2)$; ν(CN); $\omega(CH_2)$; $\rho_{op}(NH_3)$
1311sh	1312	1313	1314	1319	1322	$\nu_s(CO_2)$; ν(CN); $\omega(CH_2)$; $\rho_{op}(NH_3)$
1129	1139	1173	1175	1175	1175	ν(CN); $\omega(CH_2)$; $\rho_{ip}(NH_3)$
1109	1108	1119	1119	1117	1119	$\tau(CH_2)$; $\rho_{op}(NH_3)$
1032	1034	1016	1016	1015	1016	ν(CN)
910	923	920	921	911	914	$\rho(CH_2)$; $\omega(CO_2)$
892	892	880	880	882	882	ν(CC); $\delta(CO_2)$
687	697	712	712	711	714	$\delta(CO_2)$; δ(CCN)
606	601	588	588	584	585	$\omega(CO_2)$
502	504sh	628	630	664	662	τ(CN)
	486	477	475	482	488	$\rho(CO_2)$
	359	368	368	361	367	δ(CCN)
		246	246	255	292	libration
	199	190	191	199	239	libration
	181	171	173	158	177	libration
	165	140	147	162	157	τ(CC)
		129	129			lattice
		109	112	116	112	lattice
		69	73	73		lattice

The GVFF force constants obtained herein are not directly comparable with the force constants derived from experimental data for L-alanine, which were reported by Diem et al.,[51] who used a Urey−Bradley force field (UBFF) in order to reduce the number of adjustable parameters in their analysis. They assumed common values of force constants associated with similar bonds and angles, for example, the two CO bonds, the three methyl CH bonds, and the three ammonium NH bonds.

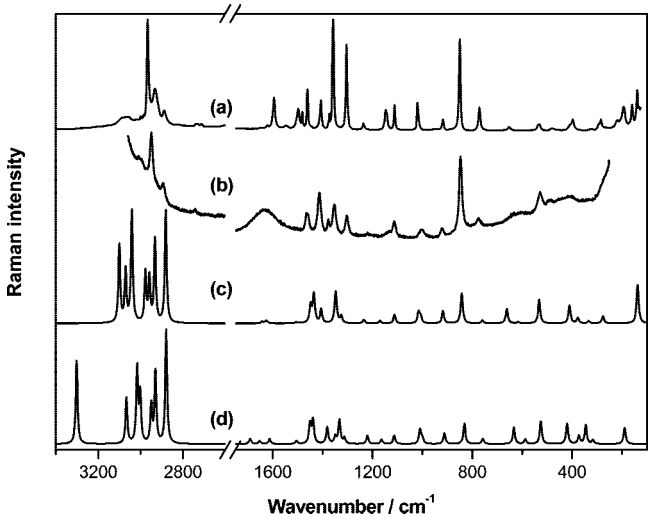

Figure 6. Raman spectrum of L-alanine in the solid state (a) and aqueous solution (b), and the simulated Raman spectra of the L-alanine model with five hydrogen-bonded water molecules models: IEF-PCM calculation (c) and gas-phase cluster calculation (d).

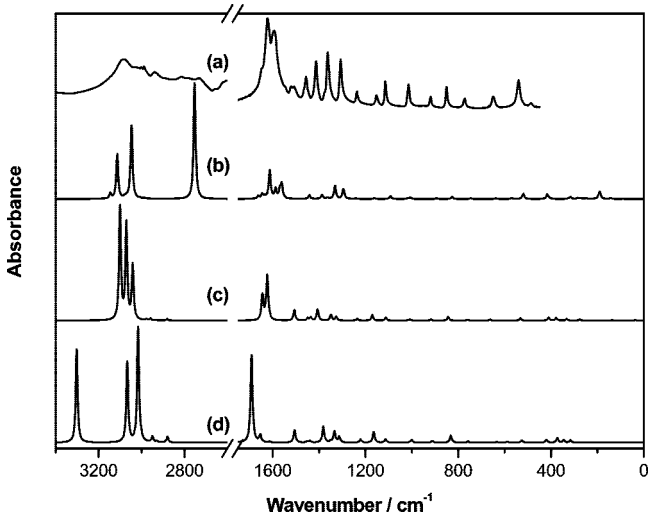

Figure 7. IR spectrum of L-alanine in the solid state (a), the simulated IR spectrum of solid L-alanine (PW91 functional) (b), and the simulated IR spectra of the L-alanine model with five hydrogen-bonded water molecules models: IEF-PCM calculation (c) and gas-phase cluster calculation (d).

The present work demonstrates that the latter assumption is invalid and that there are several discrepancies between the UBFF and GVFF force constants. Although the UBFF was popular in an era when quantum mechanical force fields were excessively computationally demanding and all normal coordinate analysis was based upon experimental vibrational spectroscopic data, the small number of force constants employed in the UBFF leads to significant error compared with the much more rigorous GVFF approach, and DFT calculations enable determination of the entire matrix of GVFF force constants.

Solid-State Vibrational Selection Rules. DFT calculations of the vibrations of glycine and L-alanine in the solid state were computed at the optimized geometries for both the PW91 and PBE functionals but were not scaled and therefore represent harmonic wavenumber values. Because the computed geometries and phonon band positions were generally better for the PW91 functional, only those results are given. As mentioned previously, the calculated optimized geometries for both amino acids had the same space groups as those determined from crystallographic data, and the solid-state vibrational selection rules are interpreted using those space groups.

The factor group for glycine is C_{2h} with four molecules per unit cell, each lying on an equivalent site of C_1 symmetry. This leads to 96 internal modes which transform as

$$\Gamma_{\text{int}} = 24a_g + 24b_g + 24a_u + 24b_u$$

Thus, each of the 24 molecular vibrations is split into four components of which two are IR active (a_u and b_u) and two are Raman active (a_g and b_g), representing the four possible phase relationships between the internal vibrations of the molecules within the unit cell. The external vibrations consist of 9 lattice modes and 12 librational modes, which transform as

$$\Gamma_{\text{lattice}} = 3a_g + 3b_g + 2a_u + b_u$$
$$\Gamma_{\text{lib}} = 3a_g + 3b_g + 3a_u + 3b_u$$

Thus, there are 3 lattice modes and 6 librational modes active in IR, and 6 of each are Raman active.

The factor group for L-alanine is D_2 with four molecules per unit cell, each lying on an equivalent site of C_1 symmetry. This leads to 132 internal modes which transform as

$$\Gamma_{\text{int}} = 33a + 33b_1 + 33b_2 + 33b_3$$

Thus, each of the 33 molecular vibrations is split into four components of which three are IR active (b_1, b_2, and b_3) and all are Raman active, and these represent the four possible phase relationships between the internal vibrations of the molecules within the unit cell. The external vibrations consist of 9 lattice modes and 12 librational modes, which transform as

$$\Gamma_{\text{lattice}} = 3a + 2b_1 + 2b_2 + 2b_3$$
$$\Gamma_{\text{lib}} = 3a + 3b_1 + 3b_2 + 3b_3$$

Thus, there are 6 lattice modes and 9 librational modes active in IR, but all are Raman active.

IR and Raman Spectra of Glycine. The solid-state and aqueous solution Raman spectra of glycine are shown in Figure 4 together with the computed spectra for the gas-phase cluster and IEF-PCM model I structures. The solid-state FTIR spectrum is shown in Figure 5 together with the computed spectra for the solid-state model (PW91 functional) and the gas-phase cluster and IEF-PCM model I. Experimental and calculated band positions with assignments are listed in Tables 7 and 8. Details for models II and III are given in the Supporting Information. The foregoing discussion relates to the results for model I, and we then discuss the differences between this and the spectra calculated for models II and III.

In the NH stretching region the gas-phase cluster calculations gave poor agreement, predicting $\nu_{as}(NH_3)$ as high as 3342 cm^{-1} and $\nu_s(NH_3)$ as low as 2673 cm^{-1}, whereas the IEF-PCM model gives values which are closer to their experimental counterparts, albeit with a much smaller wavenumber separation between symmetric and antisymmetric stretches. This is due to computed interaction force constants being too small. In the solid-state calculations it was noted that the ν(NH) vibrations appear to be localized, and although those associated with bonds N5H8 and N5H7 are in reasonable agreement with experimental data, the ν(N5H6) vibrations are predicted as low as ca. 2650 cm^{-1}, reflecting a much stronger hydrogen bond than is found experimentally. The predicted Raman-active factor group components for ν(N5H8) are 3128 and 3129 cm^{-1}, in good agreement with the observation of a single Raman band at 3143 cm^{-1}, and although the IR-active components are predicted at 3152 and 3182 cm^{-1}, only a single broad IR band is observed

TABLE 9: Experimental (IR and Raman) Vibrational Spectra (cm^{-1}) of L-Alanine Compared with Scaled Calculated Values for the L-Alanine−Water Cluster

IR	Raman		B3-LYP/cc-pVDZ		
solid	solid	soln	gas	IEF-PCM	assignments (% p.e.d.)
3072	3085		3302	3100	$\nu_{as}(NH_3)$ (94)
	3062		3067	3071	$\nu_{as'}(NH_3)$ (93)
3014	2999	3010	3016	3041	$\nu_s(NH_3)$ (88)
2991	2986	2995	3002	2977	$\nu_{as}(CH_3)$ (47), $\nu_{as'}(CH_3)$ (52)
	2966	2950	2949	2958	$\nu_{as}(CH_3)$ (49), $\nu_{as'}(CH_3)$ (41)
2929	2932		2930	2932	ν(CH) (91)
	2889	2894	2879	2881	$\nu_s(CH_3)$ (96)
2805					$2 \times \delta_{as}(CH_3)$
1644	1649		1691	1644	$\nu_{as}(CO_2)$ (28), $\delta_{as}(NH_3)$ (28), $\delta_{as'}(NH_3)$ (32)
1620	1621		1653	1629	$\delta_{as}(NH_3)$ (40), $\delta_{as'}(NH_3)$ (46)
1590	1595		1613	1623	$\nu_{as}(CO_2)$ (58), $\delta_{as}(NH_3)$ (20)
1520, 1505	1547, 1498		1505	1506	$\delta_s(NH_3)$ (97)
	1481		1451	1449	$\delta_{as}(CH_3)$ (34), $\delta_{as'}(CH_3)$ (41)
1455	1461	1461	1439	1436	$\delta_{as}(CH_3)$ (31), $\delta_{as'}(CH_3)$ (49)
1412	1408	1414	1381	1406	$\nu_s(CO_2)$ (40), ν(C1C4) (10), $\delta_{as}(CH_3)$ (24)
	1373	1379	1350	1349	$\delta_s(CH_3)$ (80)
1362	1359	1354	1333	1348	ρ(CH) (65)
1306	1305	1304	1313	1326	$\nu_s(CO_2)$ (12), $\rho_{ip}(NH_3)$ (11), ρ'(CH) (53)
1235	1237		1221	1235	$\rho_{op}(NH_3)$ (36), $\rho_{op}(CH_3)$ (20), ρ'(CH) (11)
1150	1147	1131	1164	1170	$\rho_{ip}(NH_3)$ (48), ρ'(CH) (15)
1114	1112	1114	1113	1112	ν(C4C9) (12), ν(CN) (27), $\rho_{ip}(CH_3)$ (30)
1014	1020	1003	1010	1016	ν(C4C9) (43), $\rho_{op}(NH_3)$ (20), $\rho_{op}(CH_3)$ (10)
			1000	1007	ν(CN) (15), ρ_{op} (NH_3) (10), $\rho_{ip}(CH_3)$ (25), $\rho_{op}(CH_3)$ (16)
918	918	922	912	918	ν(C1C4) (17), ν(CN) (25), $\rho_{ip}(CH_3)$ (12), $\rho_{op}(CH_3)$ (25)
850	851	848	832	843	$\nu_s(CO_2)$ (11), ν(C1C4) (11), ν(C4C9) (13), ν(CN) (15), $\delta(CO_2)$ (33)
771	772	777	759	760	δ(CCC) (11), $\omega(CO_2)$ (68)
646	653		634	662	ν(C1C4) (17), δ(C1C4N) (18), $\delta(CO_2)$ (34), $\rho(CO_2)$ (10)
539	534	529	526	532	ν(C1C4) (16), ν(CN) (14), δ(C9C4N) (16), $\rho(CO_2)$ (29)
482	480	493	588	615	τ(CN) (93)
	412	398	420	411	δ(C9C4N) (70)
	293		373	378	δ(C1C4N) (30), δ(CCC) (12), $\rho(CO_2)$ (33),τ(C4C9) (18)
	285		346	333	τ(C4C9) (80)
	221		317	277	δ(C1C4N) (16), δ(CCC) (58), $\omega(CO_2)$ (15)
			190	138	τ(C1C4) (99)

at 3160 cm^{-1}. Similarly, only single bands are observed in the IR and Raman for ν(N5H6) at 3006 and 3008 cm^{-1}, respectively, which compares favorably with the prediction of the a_g, b_g, and a_u components (all 2971 cm^{-1}), although the b_u component is predicted to be 23 cm^{-1} higher and have greater IR intensity.

The ν(CH) region is much more straightforward to assign since two bands are observed in the IR spectrum at 2962 and 2892 cm^{-1}, which correspond closely to the positions predicted for the $\nu_{as}(CH_2)$ and $\nu_s(CH_2)$ modes from the IEF-PCM model. Only the $\nu_s(CH_2)$ mode is observed in the Raman spectrum. For the gas-phase cluster model these bands are computed at positions ca. 45 cm^{-1} higher using the same CH scaling factor, and it is somewhat surprising that the hydrophobic CH_2 group should be significantly perturbed by solvation. In the solid-state calculation the $\nu(CH_2)$ bands are ca. 100 cm^{-1} higher because no scaling has been applied and the computed band positions are therefore not adjusted for anharmonicity, which is significant for vibrations involving motion of hydrogen atoms. However, the computed 80 cm^{-1} separation between $\nu_{as}(CH_2)$ and $\nu_s(CH_2)$ is in good agreement with that observed in the IR spectrum (70 cm^{-1}). There appears to be no coupling between CH and NH stretching motion, in contrast with the assignments reported by Gontrani et al.[16] in their B3-LYP/6-31G(d)/PCM calculations, but in good agreement with the findings of Tortonda et al.[17] in their B3-PW91/6-31+G(d,p) calculation in which they accounted for solvation using the continuum model of Rivail.[52]

For both the solution and solid-state models there is strong coupling between $\nu_{as}(CO_2)$ and $\delta_{as}(N_3)$. The assignments in this region are in agreement with those of Tortonda et al.[17] but contradict those of other studies in which it is claimed that $\nu_{as}(CO_2)$ and $\delta_{as}(NH_3)$ are uncoupled. Gontrani et al.[16] assign a band at 1634 cm^{-1} (1612 cm^{-1} in our work) to $\nu_{as}(CO_2)$, whereas Derbel et al.[25] attribute this mode to the lower wavenumber band at 1599 cm^{-1} (1589 cm^{-1} in this work). Those authors also disagree on the assignment of $\delta_s(NH_3)$; Gontrani et al.[16] assign a band at 1440 cm^{-1} (1445 cm^{-1} in this work) to $\delta_s(NH_3)$, which is clearly too low, and we assign that band to $\delta(CH_2)$ in agreement with Tortonda et al.[17] and Derbel et al.[25]

For both the solution model and solid-state calculations the NH_3 rocking modes are found to be substantially mixed with other types of motion, especially wagging and torsion of the CH_2 group, in agreement with previous assignments.[16,17,25] Surprisingly, the computed positions of the NH_3 deformation and rocking modes in the solid-state calculations are mostly not very much higher than their experimental values, and this may represent a cancelation of errors in the DFT calculations.

Vibrations of the CH_2 group are also readily assigned from the calculated spectra and largely in agreement with the assignments of Tortonda et al.[17] For both solution and solid-state models the CH_2 deformation is uncoupled, although CH_2 wagging, twisting, and rocking are all coupled with other types of motion, especially NH_3 rocking. The CO_2 symmetric stretch is distributed over two modes, observed in both IR and Raman, at ca. 1400 and 1330 cm^{-1}. In the higher wavenumber vibration it is coupled with CC stretching and CH_2 deformation and wagging, and in the lower it is coupled with CH_2 wagging. For

TABLE 10: Solid-State IR and Raman Spectra (cm^{-1}) of L-Alanine Compared with Calculated Values for L-Alanine in the Solid State Using the PW91 Functional

		calcd PW91				
IR solid	Raman solid	*a*	b_1	b_2	b_3	assignments
3072	3085	3106	3145	3113	3118	ν(N5H8)
	3062	3023	3047	3045	3053	ν(N5H7)
3014	2999	2738	2746	2757	2753	ν(N5H6)
2991	2986	3079	3080	3080	3079	$\nu_{as}(CH_3)$
	2966	3067	3070	3070	3068	$\nu_{as'}(CH_3)$
2929	2932	3007	3007	3007	3007	ν(CH)
	2889	2989	2986	2986	2989	$\nu_s(CH_3)$
2805						$2 \times \delta_{as}(CH_3)$
1644	1649	1663	1665	1661	1664	$\delta_{as}(NH_3)$
1620	1621	1636	1645	1642	1634	$\delta_{as'}(NH_3)$
1590	1595	1579	1612	1569	1587	$\nu_{as}(CO_2)$; $\delta_s(NH_3)$
1520,1505	1547,1498	1539	1554	1561	1552	$\delta_s(NH_3)$; $\nu_{as}(CO_2)$
	1481	1450	1471	1470	1443	$\delta_{as'}(CH_3)$
1455	1461	1445	1440	1441	1450	$\delta_{as}(CH_3)$
1412	1408	1383	1386	1388	1387	$\delta_s(CH_3)$; ρ(CH)
	1373	1365	1370	1369	1363	$\delta_s(CH_3)$; ρ(CH)
1362	1359	1332	1332	1330	1331	$\nu_s(CO_2)$; ν(C1C4); ν(C4C9)
1306	1305	1289	1293	1299	1295	ρ'(CH)
1235	1237	1239	1241	1243	1242	$\rho_{op}(NH_3)$; $\rho_{op}(CH_3)$
1150	1147	1150	1161	1160	1150	ν(CN); $\rho_{ip}(NH_3)$
1114	1112	1088	1088	1091	1092	ν(CN); $\rho_{op}(CH_3)$
1014	1020	1017	1017	1019	1019	ν(C4C9)
		1002	1006	1006	1007	ν(CN); $\rho_{op}(CH_3)$
918	918	891	894	896	893	ν(C1C4); $\rho_{ip}(CH_3)$
850	851	829	828	824	826	$\delta(CO_2)$; ν(CN); ν(C1C4)
771	772	748	750	745	747	$\omega(CO_2)$
646	653	642	639	635	639	$\rho(CO_2)$; δ(CCN)
539	534	512	517	523	520	$\rho(CO_2)$; δ(CCN)
482	480	563	570	568	562	τ(CN)
	412	401	406	413	417	δ(CCN)
	293	258	325	316	285	$\rho(CO_2)$
	285	315	259	252	316	τ(C4C9)
	221	288	276	271	248	δ(CCC)
	193	184	204	190	212	lattice
	161	156	195	163	159	libration
		149	144	142	144	libration
		115	93	127	130	τ(C1C4)
		73	105	90	111	libration
		29	31	49	55	lattice
		44*i*				lattice

both the solution and solid-state models the CN stretch is attributable to a band which appears in the IR at 1032 cm^{-1} and in the Raman at 1034 cm^{-1}. This is not significantly coupled with any other vibrational motion, unlike the CC stretch which for the solution-phase IEF-PCM model is shown to contribute to vibrations ranging from 600 to 1400 cm^{-1}.

The low-wavenumber bands can be assigned to vibrations which are mostly of mixed character involving various deformation, wagging, rocking, and torsional motions. Predicted band positions for both solution and solid are in good agreement with experimental data with one notable exception. The band which appears as a shoulder in the solid-state Raman spectrum at 504 cm^{-1} is assigned to a vibration for which the dominant component is τ(CN). In the solution-phase IEF-PCM model this vibration is predicted at 563 cm^{-1} and in the solid-state calculation is predicted to have factor-group components ranging from 628 to 664 cm^{-1}. Such a discrepancy reflects an excessive rigidity of the NH_3 group in these models. Although the gas-phase cluster model provides a more accurate prediction (491 cm^{-1}), this is considered to be fortuitous in that this model generally yields a poorer fit to the observed IR and Raman spectra. Our assignment of τ(CN) is not in agreement with previous work where lower values were computed (262 cm^{-1} [16] and 316 cm^{-1} [17]). However, we believe that the Raman band observed at 359 cm^{-1} is more reasonably assigned to the mode involving CCN deformation and CO_2 wagging, predicted at 341 cm^{-1} in the IEF-PCM model. Two low-wavenumber bands in the solid-state Raman spectrum at 181 and 199 cm^{-1} are assigned to librational modes. Various other librational and lattice modes are predicted but not observed. Finally, the three acoustic modes for glycine were calculated to be 45*i* (a_u), 24*i*, and 77 cm^{-1} (b_u).

The computed band wavenumbers from the IEF-PCM calculations for models II and III (Table S3, Supporting Information) differ in a number of ways from model I. For models II and III the $\nu_{as}(NH_3)$ vibrations are closer to the experimental values but the $\nu_s(NH_3)$ vibration is further, compared with model I. In the $\nu(CH_2)$ region models II and III predict a smaller separation between ν_{as} and ν_s (53−54 cm^{-1}) than is predicted by model I (74 cm^{-1}), which is close to the experimental value of 70 cm^{-1}. On the other hand, models II and III predict a greater difference between the wavenumbers of bands attributed vibrations involving ν_{as}(CO) and ν_s(CO) motions. As mentioned previously, this is a consequence of the greater difference in CO bond distances for these models and one of the principal reasons why we favor model I despite its higher energy. The computed positions for models II and III of other vibrations in the 800−1500 cm^{-1} region generally give a poorer fit than model I, and in the low-wavenumber region computed positions are generally too high.

IR and Raman Spectra of L-Alanine. The solid-state and aqueous solution Raman spectra of L-alanine are shown in Figure 6 together with the computed spectra for the gas-phase cluster and IEF-PCM models, and the solid-state FTIR spectrum is shown in Figure 7 together with the computed spectra for the solid-state model (PW91 functional) and the gas-phase cluster and IEF-PCM model I. Experimental and calculated band positions with assignments are listed in Tables 9 and 10. Details for models II and III are given in the Supporting Information, Table S4. The foregoing discussion relates to the results for model I, and we then discuss the differences between this and the spectra calculated for models II and III. Assignments are mostly in agreement with those of Tortonda et al.[17] and Diem,[51] although these authors do not provide p.e.d.s and list only the principal contribution to each vibration.

In the NH stretching region the gas-phase cluster calculations gave poor agreement, predicting $\nu_{as}(NH_3)$ as high as 3302 cm^{-1}, although the IEF-PCM model gives values in good agreement with experimental data. As for glycine it was found that in the solid-state calculations the ν(NH) vibrations appear to be localized and ν(N5H6) is predicted to be very low (ca. 2750 cm^{-1}). There is generally good agreement between experimental data and the calculated band positions in the CH stretching region. Only two bands are observed in the IR spectrum at 2991 and 2929 cm^{-1}, which are assigned to the high-wavenumber component of $\nu_{as}(CH_3)$ and ν(CH), respectively, whereas all four of the CH stretches are observed in the Raman spectrum. It is in this region that our assignments differ from those reported previously.[17,51] We assign the Raman band at 2966 cm^{-1} to $\nu_{as}(CH_3)$, the band at 2932 cm^{-1} to ν(CH), and the band at 2889 cm^{-1} to $\nu_s(CH_3)$. The justification for this is that both the solution-phase and solid-state DFT calculations predict these modes in that order. An additional weak band at 2805 cm^{-1} in the IR spectrum has previously[49] been assigned to the overtone of the $\delta_{as}(CH_3)$ fundamental at 1455 cm^{-1}.

In both the solution-phase and solid-state DFT calculations it is shown that the $\nu_{as}(CO_2)$ and $\delta_s(NH_3)$ motions are strongly coupled and that the NH_3 rocking motions are substantially mixed with other types of motion, especially CH_3 rocking and

CN stretching. As for glycine, the computed positions of the NH_3 deformation and rocking modes in the solid-state calculations are (mostly) not very much higher than their experimental values. Bending vibrations of the CH and CH_3 groups are also readily assigned from the calculated spectra. For both solution and solid-state models the CH_3 deformations are largely uncoupled, although in the solid-state model the symmetric CH_3 stretch is found to be coupled with CH rocking. The CO_2 symmetric stretch is distributed over two modes, observed in both IR and Raman, at ca. 1410 and 1305 cm^{-1}, and coupled with CC stretching and various rocking motions. By contrast with glycine, the DFT calculations indicate that CN stretching is distributed over four modes. The calculated positions for the IEF-PCM model are 1112, 1007, 918, and 843 cm^{-1} and in the solid state are 1150, 1088, 1002, and 829 cm^{-1} for the a_g components. These are all observed in both the IR and Raman spectra, although one of these bands is overlapped by another, whose assignment is to a mode involving mainly C4C9 stretching, giving a single broad band at 1014 cm^{-1} in the IR spectrum and 1020 cm^{-1} in the Raman spectrum of L-alanine in the solid sate.

The low-wavenumber bands can be assigned to vibrations which are mostly of mixed character involving various deformation, wagging, rocking, and torsional motions. In common with the glycine spectra, predicted band positions for both solution and solid are in good agreement with experimental data with the exception of the τ(CN) mode. This is attributed to a band at 482 cm^{-1} in the IR spectrum and 480 cm^{-1} in the solid-state Raman spectrum. In the solution-phase IEF-PCM model this vibration is predicted at 615 cm^{-1}, and in the solid-state calculation it is predicted to have factor-group components ranging from 562 to 570 cm^{-1}. Again, the difference between calculated and experimental values is attributed to excessive rigidity of the NH_3 group in both the solution and solid-state models. Two low-wavenumber bands in the solid-state Raman spectrum at 151 and 193 cm^{-1} are assigned to a librational mode and a lattice mode, respectively. Various other librational and lattice modes and the τ(C1C4) mode are predicted at lower wavenumber but not observed. Finally, the three acoustic modes for L-alanine were calculated to be 81*i* (b_2), 52*i* (b_1) and 50*i* cm^{-1} (b_3).

The computed band wavenumbers from the IEF-PCM calculations for models II and III (Table S4, Supporting Information) differ in a number of ways from model I. Models II and III yield $\nu(NH_3)$ band wavenumbers which are closer to the experimental values, but the $\nu(CH_3)$ and ν(CH) positions deviate further from their experimental values than for model I. Although model I generally yields a better fit to the experimental data, it is found that the differences between computed band positions for models I and III are not great. By contrast, model II exhibits several serious discrepancies from experimental data.

We now compare the results obtained here with those recently reported by Jalkanen et al.[39] in which they computed the Raman and ROA spectra for a L-alanine-$(H_2O)_{20}$ cluster from B3-LYP/6-31G* calculations using the COSMO[56] and Tomasi PCM[57] solvation methods. A direct comparison is not straightforward because their computed band wavenumber positions were unscaled and percent contributions for their p.e.d.s are not given. However, we are able to make a number of general observations: (i) the Raman intensity distribution in their computed spectra is poorer, most obviously in the 1500 cm^{-1} region, although this may be a consequence of the basis set rather than solvation model, (ii) they obtain the $\nu(NH_3)$ vibrations at lower wavenumber than the $\nu(CH_3)$ and ν(CH) modes, and (iii) in their COSMO calculation there is no coupling between $\nu_{as}(CO_2)$ and $\delta_{as}(NH_3)$ motions. Finally, we comment upon the computed values of vibrations involving τ(CN) motion, and we already noted that our computed value (615 cm^{-1}) is much higher than that observed (477 cm^{-1}). Jalkanen et al. obtain values of 1740, 694, and 683 cm^{-1} (PCM) and 1756 and 712 cm^{-1} (COSMO), and it therefore appears that conformational inflexibility and rigidity of the NH_3 group is even more pronounced in the L-alanine$-(H_2O)_{20}$ model.

Conclusions

In this report we have shown that the zwitterionic forms of the two simplest α-amino acids, glycine and L-alanine, in either aqueous solution or the solid state can be satisfactorily modeled by DFT calculations. Calculations of the structures in the solid state were in good agreement with the reported crystal structures, and the vibrational spectra computed at the optimized geometries provided a good fit to the observed IR and Raman spectra in the solid state, although predicted factor group splitting was generally larger than that observed. We have shown that computation of the structures and vibrational spectra of the zwitterions in aqueous solution requires both explicit and implicit solvation models. Use of an implicit solvation model alone leads to prediction of intramolecular hydrogen bonding, which does not give a satisfactory interpretation of the Raman spectrum in aqueous solution. Explicit solvation is modeled by inclusion of five hydrogen bonded water molecules, attached to each of the five possible hydrogen bonding sites in the zwitterion, but the results obtained from DFT calculations (on what is effectively a gas-phase zwitterion−water cluster) proved to be less than satisfactory in the assignment of IR and Raman spectra. However, when the geometry of the zwitterion−water cluster is optimized using the IEF-PCM model and the force constants are calculated at the optimized geometry, good agreement is found between predicted and observed spectra with one exception. The τ(CN) mode is predicted, for both amino acids, to be substantially higher than observed, and this observation is attributed to excessive rigidity of the NH_3 group in this model.

Supporting Information Available: Tables S1−S4 are auxiliary to the tables and discussion in the text. This material is available free of charge via the Internet at http://pubs.acs.org.

References and Notes

(1) Schweitzer-Stenner, R. *Vib. Spectrosc.* **2006**, *42*, 98.
(2) Carey, P. R. *J. Biol. Chem.* **1999**, *274*, 26625.
(3) Austin, J.; Rodgers, K. R.; Spiro, T. G. *Methods Enzymol.* **1993**, *226*, 374.
(4) Asher, S. A. In *Handbook of Vibrational Spectroscopy*; Chalmers, J. M., Griffiths, P. R., Eds.; Wiley: Chichester, U.K., 2001; Vol. 1, p 557.
(5) Jalkanen, K. J.; Jürgensen, V. W.; Claussen, A.; Rahim, A.; Jensen, G. M.; Wade, R. C.; Nardi, F.; Jung, C.; Degtyarenko, I. M.; Nieminen, R. M.; Herrmann, F.; Knapp-Mohammady, M.; Niehaus, T. A.; Frimand, K.; Suhai, S. *Int. J. Quantum Chem.* **2006**, *106*, 1160.
(6) Keiderling, T. In *Infrared and Raman Spectroscopy of Biological Materials*; Yan, B., Gremlich, H.-U., Eds.; Marcel Dekker: New York, 2001; pp 55−100.
(7) Pacios, L. F.; Gálvez, O.; Gómez, P. C. *J. Phys Chem. A* **2001**, *105*, 5232.
(8) Stepanian, S. G.; Reva, I. D.; Radchenko, E. D.; Rosado, M. T. S.; Duarte, M. L. R. S.; Fausto, R.; Adamowicz, L. *J. Phys Chem. A* **1998**, *102*, 1041.
(9) Kumar, S.; Rai, A. K.; Singh, V. B.; Rai, S. B. *Spectrochim. Acta* **2005**, *61A*, 2741.
(10) Selvarengan, P.; Kolandaivel, P. *J. Mol. Struct.-Theochem* **2002**, *617*, 99.
(11) Wang, W.; Zheng, W.; Pu, X.; Wong, N.-B.; Tian, A. *J. Mol. Struct.-Theochem* **2002**, *618*, 235.

(12) Tortonda, F. R.; Pascual-Ahuir, J. L.; Silla, E.; Tuñón, I. *J. Mol. Struct.-Theochem* **2003**, *623*, 203.
(13) Túlio, M.; Rosado, S.; Duarte, M. L. R. S.; Fausto, R. *J. Mol. Struct.* **1997**, *410*, 343.
(14) Stepanian, S. G.; Reva, I. D.; Radchenko, E. D.; Adamowicz, L. *J. Phys Chem. A* **1998**, *102*, 4623.
(15) Maul, R.; Ortman, E.; Preuss, M.; Hannewald, K.; Bechstedt, E. *J. Comput. Chem.* **2007**, *28*, 1817.
(16) Gontrani, L.; Mennucci, B.; Tomasi, J. *J. Mol. Struct.-Theochem* **2000**, *500*, 113.
(17) Tortonda, F. R.; Pascual-Ahuir, J.-L.; Silla, E.; Tuñón, I.; Ramirez, F. J. *J. Chem. Phys.* **1998**, *109*, 592.
(18) Almlöf, J.; Kvick, A.; Thomas, J. O. *J. Chem. Phys.* **1973**, *59*, 3901.
(19) Lehmann, M. S.; Koetzle, T. F.; Hamilton, W. C. *J. Am. Chem, Soc.* **1972**, *94*, 2657.
(20) Nóbrega, G. F.; Sambrano, J. R.; de Souza, A. R.; Queralt, J. J.; Longo, E. *J. Mol. Struct.-Theochem* **2001**, *544*, 151.
(21) Williams, R. W.; Schlücker, S.; Hudson, B. S. *Chem. Phys.* **2008**, *343*, 1.
(22) Chaudhari, A.; Lee, S.-L. *Chem. Phys.* **2005**, *310*, 281.
(23) Jensen, J. H.; Gordon, M. S. *J. Am. Chem. Soc.* **1995**, *117*, 8159.
(24) Cui, G. *J. Chem. Phys.* **2002**, *117*, 4720.
(25) Derbel, N.; Hernández, B.; Pflüger, F.; Liquier, J.; Geinguenaud, F.; Jaïdane, N.; Lakhdar, B.; Ghomi, M. *J. Phys. Chem. B* **2007**, *111*, 1470.
(26) Kassab, E.; Langlet, J.; Evleth, E.; Akacem; Y, *J. Mol. Struct.-Theochem* **2000**, *531*, 267.
(27) Wang, W.; Pu, X.; Zheng, W.; Wong, N.-B.; Tian, A. *J. Mol. Struct.-Theochem* **2003**, *626*, 127.
(28) Chaudhari, A.; Sahu, P. K.; Lee, S.-L. *J. Chem. Phys.* **2004**, *120*, 170.
(29) Williams, R. W.; Bone, I.; Weir, A. F. *J. Mol. Struct.* **2004**, *697*, 81.
(30) Ahn, D.-S.; Park, S.-W.; Jeon, L.-S.; Lee, M.-K.; Kim, N.-H.; Han, Y. H.; Lee, S. *J. Phys. Chem. B* **2003**, *107*, 14109.
(31) Chaudhari, A.; Sahu, P. K.; Lee, S.-L. *J. Mol. Struct.-Theochem* **2004**, *683*, 115.
(32) Yamabe, S.; Ono, N.; Rsuchida, N. *J. Phys Chem. A* **2003**, *107*, 7915.
(33) Tajkhorshid, E.; Jalkanen, K. J.; Suhai, S. *J. Phys. Chem. B* **1998**, *102*, 5899.
(34) Frimand, K.; Bohr, H.; Jalkanen, K. J.; Suhai, S. *Chem. Phys.* **2000**, *255*, 165.
(35) Jalkanen, K. J.; Nieminen, R. M.; Frimand, K.; Bor, J.; Bohr, H.; Wade, R. C.; Tajkhorshid, E.; Suhai, S. *Chem. Phys.* **2001**, *265*, 125.
(36) Kumar, S.; Rai, A. K.; Rai, S. B.; Rai, D. K.; Singh, A. N.; Singh, V. B. *J. Mol. Struct.* **2006**, *791*, 23.
(37) Degtyarenko, I. M.; Jalkanen, K. J.; Gurtovenko, A. A.; Nieminen, R. M. *J. Phys. Chem. B* **2007**, *111*, 4227.
(38) Degtyarenko, I. M.; Jalkanen, K. J.; Gurtovenko, A. A.; Nieminen, R. M. *J. Comp. Theor. Nanosci.* **2008**, *5*, 277.
(39) Jalkanen, K. J.; Degtyarenko, I. M.; Nieminen, R. M.; Cao, X.; Nafie, L. A.; Zhu, F,; Barron, L. D. *Theor. Chem. Acc.* **2008**, *119*, 191.
(40) Frisch, M. J.; Trucks, G. W.; Schlegel, H. B.; Scuseria, G. E.; Robb, M. A.; Cheeseman, J. R.; Montgomery, J. A., Jr.; Vreven, T.; Kudin, K. N.; Burant, J. C.; Millam, J. M.; Iyengar, S. S.; Tomasi, J.; Barone, V.; Mennucci, B.; Cossi, M.; Scalmani, G.; Rega, N.; Petersson, G. A.; Nakatsuji, H.; Hada, M.; Ehara, M.; Toyota, K.; Fukuda, R.; Hasegawa, J.; Ishida, M.; Nakajima, T.; Honda, Y.; Kitao, O.; Nakai, H.; Klene, M.; Li, X.; Knox, J. E.; Hratchian, H. P.; Cross, J. B.; Bakken, V.; Adamo, C.; Jaramillo, J.; Gomperts, R.; Stratmann, R. E.; Yazyev, O.; Austin, A. J.; Cammi, R.; Pomelli, C.; Ochterski, J. W.; Ayala, P. Y.; Morokuma, K.; Voth, G. A.; Salvador, P.; Dannenberg, J. J.; Zakrzewski, V. G.; Dapprich, S.; Daniels, A. D.; Strain, M. C.; Farkas, O.; Malick, D. K.; Rabuck, A. D.; Raghavachari, K.; Foresman, J. B.; Ortiz, J. V.; Cui, Q.; Baboul, A. G.; Clifford, S.; Cioslowski, J.; Stefanov, B. B.; Liu, G.; Liashenko, A.; Piskorz, P.; Komaromi, I.; Martin, R. L.; Fox, D. J.; Keith, T.; Al-Laham, M. A.; Peng, C. Y.; Nanayakkara, A.; Challacombe, M.; Gill, P. M. W.; Johnson, B.; Chen, W.; Wong, M. W.; Gonzalez, C.; Pople, J. A. *Gaussian03*, revision C.02; Gaussian, Inc.: Pittsburgh, PA, 2003.
(41) Becke, A. D. *J. Chem. Phys.* **1993**, *98*, 5648.
(42) Lee, C.; Yang, W.; Parr, R. G. *Phys. Rev. B* **1988**, *37*, 785.
(43) Dunning, T. H. *J. Chem. Phys.* **1989**, *90*, 1007.
(44) Cances, M. T.; Mennucci, V.; Tomasi, J. *J. Chem. Phys.* **1997**, *107*, 3032.
(45) Barone, V.; Cossi, M.; Mennucci, B.; Tomasi, J. *J. Chem. Phys.* **1997**, *107*, 3210.
(46) Clark, S. J.; Segall, M. D.; Pickard, C. J.; Hasnip, P. J.; Probert, M. J.; Refson, K.; Payne, M. C. *Z. Kristallogr.* **2005**, *220*, 567.
(47) Perdew, J. P.; Chevary, J. A.; Vosko, S. H.; Jackson, K. A.; Pederson, M. R.; Singh, D. J.; Fiolhais, C. *Phys. Rev. B* **1992**, *46*, 6671.
(48) Perdew, J. P.; Burke, K.; Ernzerhof, M. *Phys. Rev. Lett.* **1996**, *77*, 3865.
(49) Monkhorst, H. J.; Pack, J. D. *Phys. Rev. B* **1976**, *13*, 5188.
(50) Schachtschneider, J. A. *Vibrational Analysis of Polyatomic Molecules; Parts V and VI; Technical Report Nos. 231 and 57*; Shell Development Co.: Houston, TX, 1964 and 1965.
(51) Pulay, P.; Fogarasi, G.; Pang, F.; Boggs, J. E.; Vargha, A. *J. Am. Chem. Soc.* **1983**, *105*, 7037.
(52) Ugliengo, P.; Viterbo, D.; Chiari, G. *Z. Kristallogr.* **1993**, *207*, 9.
(53) Chisholm, J. A.; Motherwell, S.; Tulip, P. R.; Parsons, S.; Clark, S. J. *Cryst. Growth Des.* **2005**, *5*, 1437.
(54) Diem, M.; Polavarapu, P. L.; Oboodi, M.; Nafie, L. A. *J. Am. Chem. Soc.* **1982**, *104*, 3329.
(55) Rivail, J. L.; Rinaldi, D.; M. F. Ruiz-López, M. F. In *Theoretical and Computational Models for Organic Chemistry*; Formosinho, S. J., Arnaut, L., Csizmadia, I., Eds.; Kluwer: Dordrecht, 1991.
(56) Eckert, F.; Klamt, A. *AIChE J.* **2002**, *48*, 369.
(57) Tomasi, J.; Persico, M. *Chem. Rev.* **1994**, *94*, 2027.

JP8037945